

1 **Lacustrine leaf wax isotopes reveal strong regional climate feedbacks in**
2 **Beringia since the last ice age**

3
4 **W. C. Daniels^{1,2}, J. M Russell¹, C. Morrill^{3,4}, W. M. Longo¹, A. E. Giblin², P.**
5 **Holland-Stergar¹, J. M. Welker^{5,6}, X. Wen⁷, A. Hu⁸, Y. Huang¹**

6
7 ¹Department of Earth, Environment and Planetary Science; Brown University; 324 Brook
8 St., Providence, RI, 02912.

9 ²The Ecosystem Center; Marine Biological Laboratory; 7 MBL St., Woods Hole, MA,
10 02543.

11 ³Cooperative Institute for Research in Environmental Sciences; University of Colorado;
12 Boulder, CO, 80309.

13 ⁴National Centers for Environmental Information, NOAA, 325 Broadway, Code E/NE33,
14 Boulder, CO 80305.

15 ⁵Department of Biological Sciences, University of Alaska, Anchorage; Anchorage, AK.

16 ⁶Ecology and Genetics Research Unit, University of Oulu, Finland & UArctic.

17 ⁷Department of Atmospheric and Oceanic Sciences, Peking University; Beijing China,
18 100871.

19 ⁸Climate and Global Dynamics Laboratory, National Center for Atmospheric Research,
20 Boulder, CO 80305.

21
22 Corresponding author: William Daniels (william_daniels@alumni.brown.edu)
23
24

25 **Abstract**

26 The Late-Quaternary climate of Beringia remains unresolved despite the region's
27 role in modulating glacial-interglacial climate and as the likely conduit for human
28 dispersal into the Americas. Here, we investigate Beringian temperature change using an
29 ~32,000-year lacustrine record of leaf wax hydrogen isotope ratios (δD_{wax}) from Arctic
30 Alaska. Reconstructed temperatures were 2.9 °C colder during the Last Glacial
31 Maximum (LGM; 21-25 ka) than the pre-industrial era (PI; 2-0.1 ka). This ice-age
32 cooling is substantially smaller than in other parts of the Arctic, reflecting altered
33 atmospheric circulation and increased continentality which weakened glacial cooling in
34 the region. Deglacial warming was punctuated by abrupt events that are largely
35 synchronous with events seen in Greenland ice cores that originate in the North Atlantic
36 but which are also controlled locally, such as by the opening of the Bering Strait between
37 13.4 and 11 ka. Our reconstruction, together with climate modeling experiments,
38 indicates that Beringia responds more strongly to North Atlantic freshwater forcing under
39 modern-day, open-Bering Strait conditions than under glacial conditions. Furthermore, a
40 1.7 °C increase over the anthropogenic era reverses a 5.5 °C decline through the
41 Holocene, indicating that recent warming in Arctic Alaska has not surpassed peak
42 Holocene warmth.

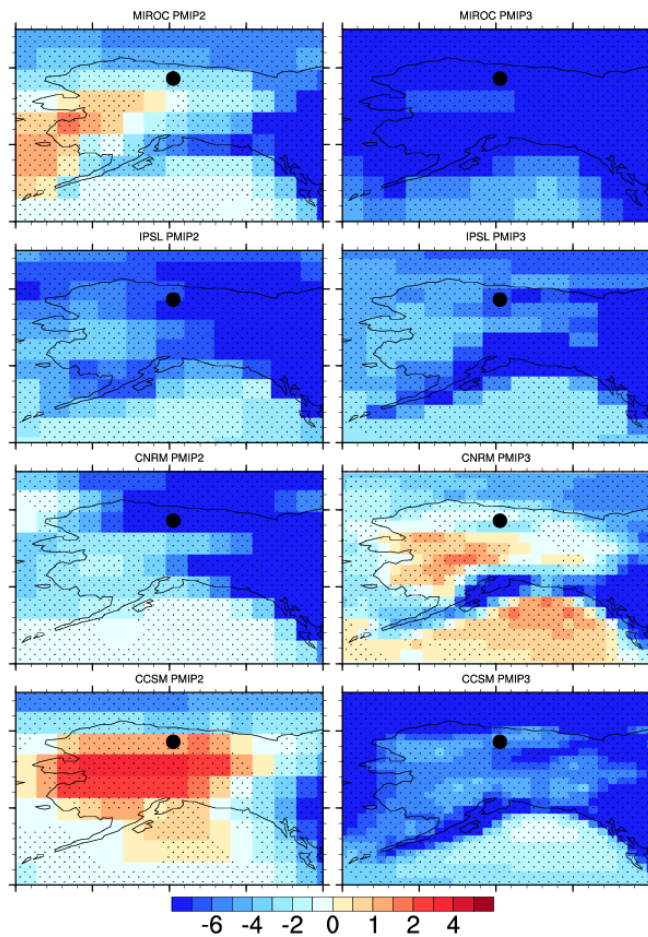
43

44 **1 Introduction**

45 During the last glacial termination, the Arctic experienced some of the most
46 extreme temperature changes known in recent geologic time. In the North Atlantic
47 region, this includes up to 23 °C of warming from 25 ka to present (Dahl-Jensen et al.,
48 1998) and high-amplitude abrupt changes such as Heinrich Stadial 1 (HS1), the Bølling-
49 Allerød (BA), and the Younger Dryas (YD) (Grootes et al., 1993; Johnsen et al., 1992;
50 Severinghaus and Brook, 1999). The magnitude and rate of these changes are linked to
51 changes in the strength of the Atlantic meridional overturning circulation (AMOC) and
52 feedbacks from sea ice (Broecker et al., 1989; Li et al., 2005) that cause temperature
53 changes to be larger than anywhere else on earth – a phenomenon known as “Arctic
54 Amplification” (Shakun and Carlson, 2010). However, Arctic paleoclimate records are
55 heavily concentrated in the North Atlantic region, which may not represent temperature

56 changes over the Arctic as a whole (Shakun and Carlson, 2010). Thus, spatiotemporal
57 variations in Arctic Amplification, and its underlying physics, remain poorly known.

58 Eastern Beringia, the region today encompassing Alaska and the Yukon Territory,
59 also experienced dramatic environmental changes during the last glacial-interglacial
60 transition. Several paleoenvironmental archives extend through the last glacial period,
61 owing to the lack of regional glaciation during the LGM. Major changes included the
62 submergence of the Bering Land Bridge, the expansion of peat soils (Jones and Yu, 2010)
63 as well as trees and shrubs (Eisner and Colinvaux, 1992; Mann et al., 2010; Oswald et al.,
64 1999), retreat of mountain glaciers (Hamilton, 2003; Pendleton et al., 2015), permafrost
65 degradation (Mann et al., 2010), the loss of megafauna (Mann et al., 2013), and the
66 appearance of humans (Goebel et al., 2008). Questions remain, however, about the
67 temperature changes during the deglacial period. Some Arctic Alaskan pollen-based
68 estimates suggest LGM temperatures were actually warmer than present (Bartlein et al.,
69 2011). Lower sea levels increased the continentality of Alaska and may have weakened
70 summertime cooling in parts of Beringia (Bartlein et al., 2015; Mann et al., 2001).
71 Climate models further predict that Laurentide Ice Sheet (LIS) orography steered warm
72 air into Alaska during the LGM maintaining relatively mild or even warmer temperatures
73 relative to the present (Bartlein et al., 2011; Broccoli and Manabe, 1987; Otto-Bliesner et
74 al., 2006; Tierney et al., 2020). However, pollen-based temperature reconstructions are
75 limited because Pleistocene ecosystems of Beringia have no modern analog, while
76 different climate models predict different, and often opposite, temperature changes in
77 Arctic Alaska in response to changes in LIS height (Figure 1), calling this mechanism
78 into question.



79

80 **Figure 1.** Multi-model simulations of LGM mean annual temperature change in Alaska
 81 (LGM-PI) under PMIP2 (left) and PMIP3 (right) boundary condition scenarios. The
 82 black dot represents location of Lake E5. These results highlight the variability among
 83 models in their sensitivity to the Laurentide Ice Sheet configuration, as this was one of
 84 the key differences in boundary conditions for the Beringia region between the two
 85 model generations. Stippling indicates anomalies that are statistically significant at the
 86 $p=0.05$ level according to a t-test.

87

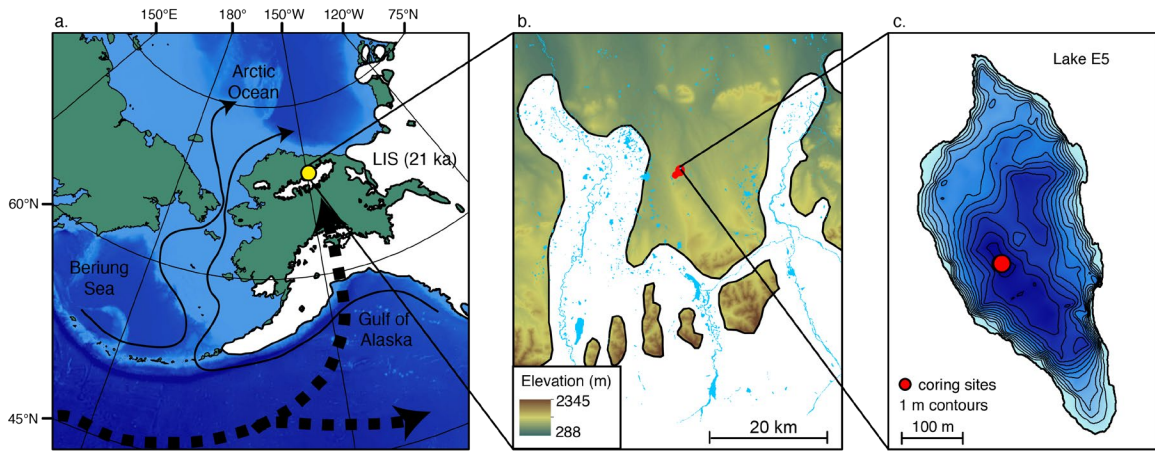
88 Within the last glacial termination, much of the Arctic experienced abrupt climate
 89 events associated with Heinrich Stadial 1 (HS1), the Bølling-Allerød (BA), and the
 90 Younger Dryas (YD). In Eastern Beringia, evidence for BA-YD climate reversals is
 91 found in both marine (Praetorius and Mix, 2014) and terrestrial records (Engstrom et al.,
 92 1990; Epstein, 1995; Mann et al., 2002; Meyer et al., 2010; Young et al., 2019), although
 93 several locations show no YD signal (Kurek et al., 2009b). The magnitude of temperature
 94 changes during these abrupt transitions is not tightly constrained in Alaska, but is thought

95 to be weaker than in the North Atlantic (Graf and Bigelow, 2011; Hu et al., 2006). In
96 addition to these millennial-scale events, resubmergence of the Bering land bridge and
97 establishment of Bering Strait throughflow between 13.4 ka and 11.0 ka (England and
98 Furze, 2008; Jakobsson et al., 2017; Keigwin et al., 2006; Pico et al., 2020) likely had
99 considerable influence on local Beringia climate. Sites adjacent to the Bering Strait
100 cooled in summer and warmed in winter in response to an increasingly maritime climate
101 (Bartlein et al., 2015; Mann et al., 2001), although the spatial ramifications of this
102 transition are unconstrained. This effect may have been partially offset by the initiation of
103 north-flowing ocean currents and heat transport from the North Pacific into the Western
104 Arctic, warming broader Beringia (Hu et al., 2012), although this hypothesis requires
105 more investigation. Bering Strait status is also proposed to modulate the North Pacific
106 circulation response to deglacial freshwater release events in the North Atlantic (Hu et
107 al., 2012). For example, during HS1 (~15-18 ka), collapse of AMOC is associated with
108 an invigoration of Pacific Meridional Oceanic Circulation (PMOC) (Maier et al., 2018;
109 Okazaki et al., 2010), minimizing or even reversing temperature changes in the North
110 Pacific relative to the North Atlantic (Sarnthein et al., 2006). Warm sea surface
111 temperatures during HS1 may have influenced continental Beringia, as suggested by
112 chironomid-inferred warming from 17-14 ka at Zagoskin Lake in Alaska (Kurek et al.,
113 2009a), although more records are needed to confirm this.

114 Here, we generate a centennially-resolved record of temperature change from the
115 northern foothills of the Brooks Range mountains (68.643 °N, 149.458 °W, Figure 2) to
116 examine the amplitude and causes of temperature changes from Arctic Alaska during the
117 LGM, the last deglaciation, and the Holocene. This new dataset, alongside paleoclimate
118 data-model comparisons, provide new insight into the large-scale and regional controls
119 on temperature change in this part of the Arctic.

120

121 **2 Materials and Methods**



122

123 **Figure 2.** a) Map of Beringia with ice extent 21,000 calendar years before present (21 ka)
 124 (Dyke, 2004) and E5 study lake (yellow dot). Bold dashed arrows represent the LIS-
 125 orography forced northward advection of subpolar air into Alaska as simulated in
 126 CCSM3 (Otto-Bliesner et al., 2006). Solid arrows are modern surface currents through
 127 the Bering Strait (Stabeno et al., 1999). b) study area showing surface waters, the Lake
 128 E5 watershed (red), and the maximum glacier extent of the late-Wisconsin glaciation
 129 (Manley and Kaufman, 2002). c) Lake E5 bathymetry (Toolik GIS, 2019) and coring
 130 sites.

131

132 2.1 Lake Setting and Core Chronology

133 Lake E5, located in Alaska's North Slope (Figure 2), is a glacial lake containing
 134 sediments extending through the LGM (Eisner and Colinvaux, 1992), providing an
 135 extraordinary opportunity to examine deglacial climate change in the Western Arctic.
 136 Meteorological observations at the nearby Toolik Field Station, approximately 5 km to
 137 the west, show that mean annual temperature averages -8.5°C , summer temperatures
 138 (JJA) average 9°C , and precipitation averages 312 mm with 60% falling during summer
 139 (Cherry et al., 2014).

140 The study lake is situated on glacial deposits dating to 780-125 ka (Hamilton,
 141 2003). It is 12 m deep and typically ice-free from early June to mid-September. Gravity
 142 cores were retrieved from a boat in 2011 and 2012, and in May, 2014, overlapping
 143 sediment cores were recovered using a Bolivia and modified Livingstone square-rod
 144 piston corer through the ice from the deepest point in the lake. The composite core is 4.8
 145 m long, consisting of laminated to thinly bedded silts and clays (Supplemental Text,
 146 Figures S1 to S3).

147 An age model (Longo et al., 2020; Vachula et al., 2019) was constructed from
148 ^{210}Pb and 16 radiocarbon dates including ultra-microscale ^{14}C analyses (Shah Walter et
149 al., 2015) of plant or insect fragments, and in some cases a mixture of the two
150 (Supplemental Text, Table S1 and S2, Figure S2). Ages were modeled using Clam
151 version 2.2 (Blaauw, 2010; Reimer et al., 2013). The lowest radiocarbon sample dates to
152 $28,488 \pm 1001$ (1σ) calendar years before present, and extrapolation of the lower
153 sedimentation rate produces a basal date of $32,086 \pm 2197$ (2σ) cal. yr BP. The 95%
154 confidence interval ranges from ± 4 years at the core top to ± 2208 years at the base, and
155 averages ± 810 years throughout the entire record. The age model is less-tightly
156 constrained within the last glacial period.

157

158 2.2 Leaf Wax Hydrogen Isotope Analysis

159 Hydrogen isotope ratios of terrestrial leaf waxes (C_{28} *n*-acid; hereafter $\delta\text{D}_{\text{wax}}$)
160 were measured in Lake E5 sediments as a proxy for changes in past $\delta\text{D}_{\text{precipitation}}$ and
161 climate. Lipids were extracted from 1-5 g of dry sediment using a Dionex accelerated
162 solvent extractor with 9:1 dichloromethane:methanol. Total lipid extracts were separated
163 using aminopropyl silica gel chromatography with 2:1 dichloromethane:isopropanol and
164 4% acetic acid in ether as eluents. Acid fractions were then methylated overnight at $60\text{ }^{\circ}\text{C}$
165 in acidified methanol of known isotopic composition. Further purification of fatty acid
166 methyl esters (FAMES) was performed with silica gel chromatography with
167 dichloromethane and hexane as eluents.

168 Hydrogen isotope ratios of FAMES were analyzed on a Thermo Finnegan Delta
169 XL GC-IRMS at Brown University. Each sample was injected at least twice, targeting the
170 *n*- C_{28} acid to be in the range of 3-5 volts. The δD values are reported relative to VSMOW
171 in delta notation, and analytical uncertainties are reported in Table S3. $\delta\text{D}_{\text{wax}}$ values are
172 mathematically corrected for the methyl groups added during derivatization.

173

174 2.3. Temperature estimation

175 Previous quantitative reconstructions of $\delta\text{D}_{\text{precipitation}}$ from measurements of $\delta\text{D}_{\text{wax}}$
176 have demonstrated the need to account for glacial-interglacial changes in oceanic D/H
177 ratios (Konecky et al., 2016). We correct for this effect across the last glacial termination

178 by subtracting the δD_{ocean} anomaly from the measurements of δD_{wax} . The δD_{ocean} anomaly
179 is determined by assuming LGM ocean was 1‰ enriched in $\delta^{18}\text{O}$ relative to today
180 (Schrag et al., 1996), scaling the 1‰ glacial-interglacial change to the foramanifera-
181 inferred changes in $\delta^{18}\text{O}$ (Lisiecki and Raymo, 2005), then converting to δD by
182 multiplying by 8.

183 Additionally, to estimate changes in $\delta D_{\text{precipitation}}$ through time at Lake E5 from
184 δD_{wax} , we apply a vegetation correction to the δD_{wax} data using landscape-scale
185 fractionation values determined through local water and plant isotope monitoring studies
186 (Daniels et al., 2017) applied to previously documented pollen spectra from Lake E5
187 (Eisner and Colinvaux, 1992) (Figure S4). This assumes that the leaf wax compounds are
188 derived from land plants, and indeed the C_{28} *n*-acid is commonly produced by terrestrial
189 plants (Chikaraishi and Naraoka, 2007) and is geochemically stable in sediments (Yang
190 and Huang, 2003). While long chain ($>C_{24}$) *n*-acids can also be produced by aquatic
191 plants, the extremely oligotrophic status of Lake E5 (Daniels et al., 2015) suggests that
192 terrestrial sources dominate. Determination of $\delta D_{\text{precipitation}}$ from δD_{wax} is improved by
193 accounting for changes in terrestrial plant composition (Feakins, 2013; Konecky et al.,
194 2016), as the D/H fractionation between water and lipids (ϵ_{app}) varies among plant types
195 (Daniels et al., 2018; Daniels et al., 2017; Gao et al., 2014; Sachse et al., 2012).

196 Generally, monocotyledonous plants fractionate more strongly than dicotyledonous
197 plants. As the ratio of these plant types has fluctuated in the Lake E5 region between the
198 LGM and today (Eisner and Colinvaux, 1992), so too has the ecosystem scale value of
199 ϵ_{app} . In general, the Holocene is characterized by greater abundance of dicot shrubs,
200 particularly of the genera *Betula*, *Salix*, and *Alnus*, whereas during the LGM, grasses
201 (*Poaceae*) were relatively abundant (Abbott et al., 2010; Eisner and Colinvaux, 1992;
202 Livingstone, 1955). During the glacial termination, transient peaks in *Artemesia* and
203 sedges of the *Cyperaceae* family are evident around 16 and 11-15 ka, respectively
204 (Abbott et al., 2010; Eisner and Colinvaux, 1992).

205 To account for these changes, we performed a vegetation correction based on the
206 pollen stratigraphy from a previous published record from Lake E5 (Eisner and
207 Colinvaux, 1992). Such corrections are likely imperfect because of uncertainty in the
208 pollen-wax production ratios among different plants. Nonetheless, this approach has been

209 used previously with success (Feakins, 2013) and improved estimates of the effect of
210 vegetation on ϵ_{app} are available from the Arctic (Berke et al., 2019; Daniels et al., 2017;
211 Wilkie et al., 2012). The Eisner-Colinvaux core was depth-correlated to our stratigraphy
212 based on organic carbon profiles and a distinct marker bed dating to the beginning of the
213 deglaciation. Based on a 24-lake training set in the Alaskan tundra (Daniels et al., 2017),
214 we determined that lakes in watersheds with a predominance of wet sedge tundra or
215 grasses exhibit ϵ_{app} of -135 ($1\sigma = 20\text{‰}$), whereas forb/shrub-dominated tundra have ϵ_{app}
216 of -96 ($1\sigma \approx 16\text{‰}$), relative to source water D/H ratios. We generate a mixing model
217 using these two endmembers and the fraction of monocot and dicot pollen to calculate
218 ϵ_{app} for each time point in the data series. From this, we calculated $\delta D_{\text{precipitation}}$ (Figure
219 S4).

220 To estimate temperature from $\delta D_{\text{precipitation}}$, we use the temperature- $\delta D_{\text{precipitation}}$
221 relationship determined from 20 years of precipitation monitoring at the Toolik Field
222 Station, approximately 5 km west of and at a similar elevation to Lake E5. Over the 20
223 years of monitoring, precipitation sampling was opportunistic and sporadic, depending on
224 the availability of the researchers; specific events were neither targeted nor avoided. We
225 tested the δD -temperature relationship further using isotope enabled climate simulations.
226 An isotope-enabled version of the Community Atmosphere Model (IsoCAM) was
227 employed to examine changes in the slope of the $\delta D_{\text{precipitation}}$ -T relationship at 1000 year
228 time slices over the past 20 kyr in Alaska, as the relationship between these variables
229 might be expected to change with major moisture source changes (Liu et al., 2014;
230 Tharammal et al., 2013; Thomas et al., 2014). Monthly temperatures were extracted from
231 each time slice for 40 years from 6 grid cells that cover Northern Alaska, and we
232 analyzed the relationship between temperature and $\delta D_{\text{precipitation}}$ on these data.

233 All vegetation corrections and temperature conversions were performed in a
234 monte-carlo simulation in order to propagate uncertainty estimates of the δD_{wax}
235 measurements (average $1\sigma = 1.3\text{‰}$, Table S3), the pollen-inferred vegetation
236 assemblages (ie. fraction monocot and fraction dicot; 1σ prescribed at 0.05), D/H
237 fractionation endmember values (uncertainty reported above), and the temperature-
238 $\delta D_{\text{precipitation}}$ relationship. Monte carlo simulations were performed using 1000 iterations.
239 To assess temperature changes between discrete time slices, we performed two-tailed

240 Student's t-tests on the monte carlo distributions after compositing results for each time
241 point within the periods of interest.

242

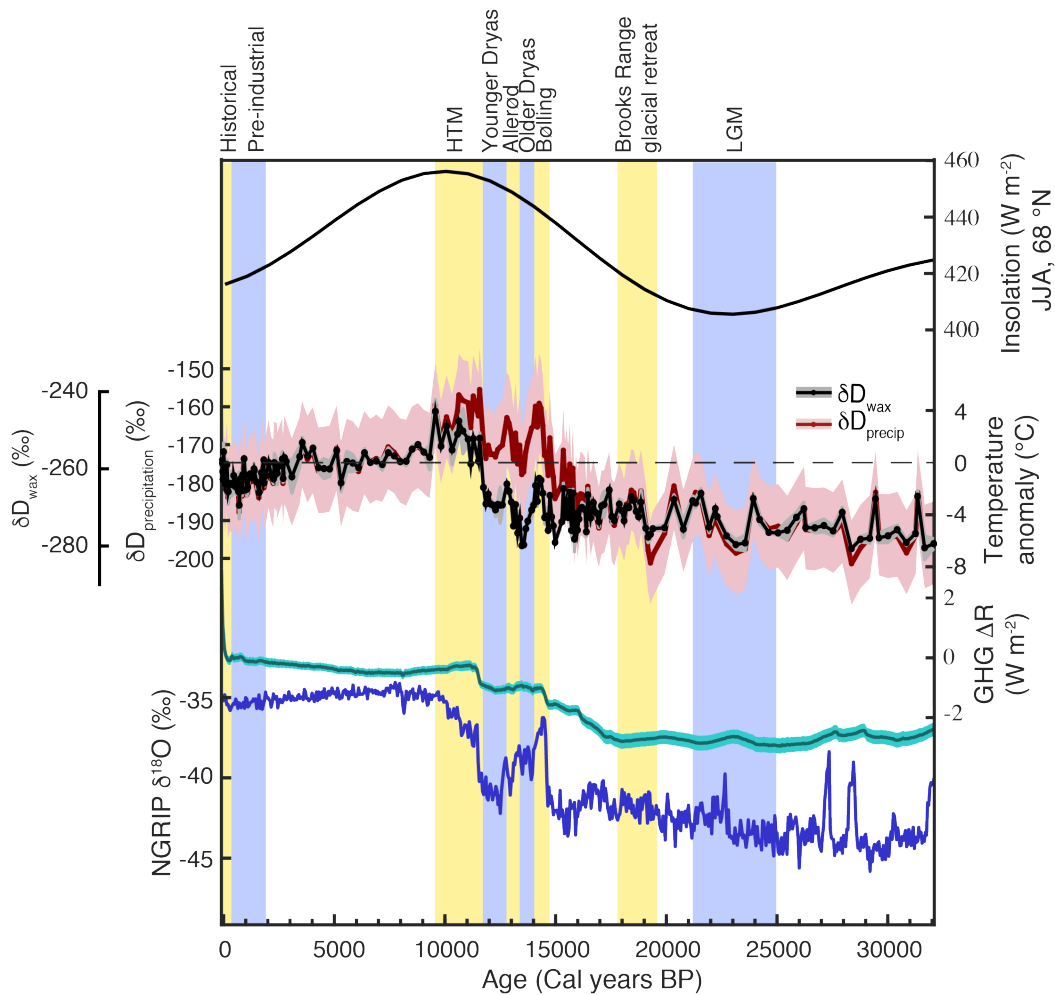
243 2.4 Climate Model Simulations

244 We use the Community Climate System Model 3 (CCSM3) global circulation
245 model to test the effect of Bering Strait opening/closure and other glacial/interglacial
246 boundary conditions on Beringian temperature and on Beringian sensitivity to global
247 freshwater forcing events. The model has fully-coupled atmosphere, land, ocean, and sea
248 ice components with a horizontal resolution of T42 or 2.8 degrees for atmospheric and
249 land models and nominal 1 degree with enhanced meridional resolution to 1/3 degree in
250 the equatorial tropics for the ocean and sea ice models. Boundary conditions are provided
251 by Hu et al. (2015) and include changes to the Laurentide Ice Sheet, orbital forcing, and
252 atmospheric greenhouse gas concentrations. Surface temperatures were averaged over
253 100 years under 15 ka boundary conditions with an open and closed Bering Strait, and
254 under present-day (1990 A.D.) boundary conditions with an open and closed Bering
255 Strait. The model scenarios are idealized and not meant to represent the exact conditions
256 under which the Bering Strait was flooded. Additionally, the same model configurations
257 are used to test the effect of freshwater addition to the North Atlantic on Beringian
258 climate. Under the four scenarios described above (15 ka open/closed, 0 ka open/close),
259 freshwater was gradually added to the North Atlantic until the AMOC collapsed, at which
260 point surface temperatures from Beringia for the succeeding 100 years were averaged.

261

262 **3 Results**

263 3.1 *n*-acid distributions, D/H ratios, and vegetation correction



264

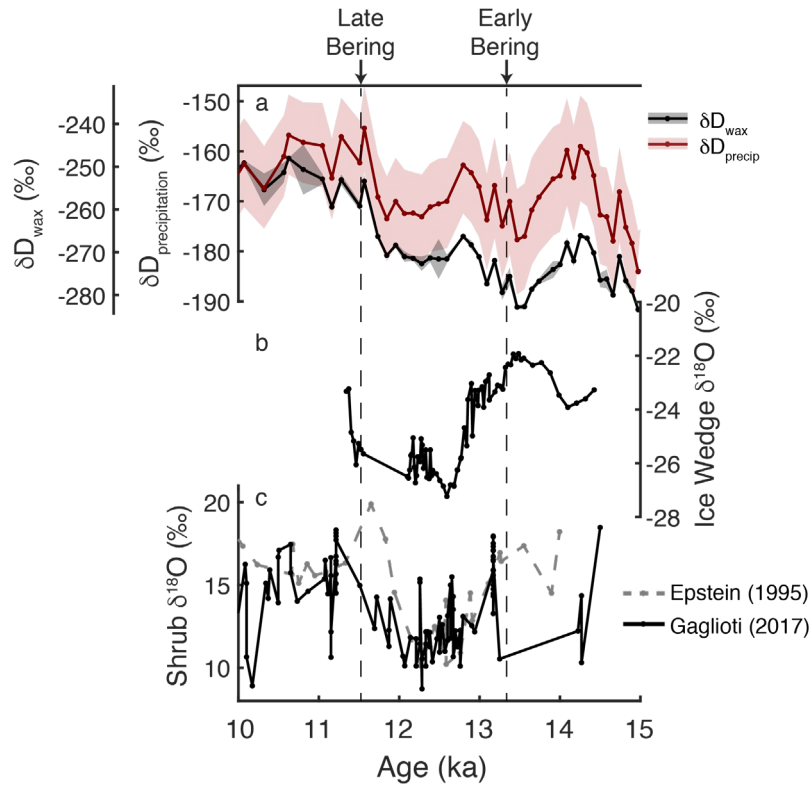
265 **Figure 3.** Leaf wax hydrogen isotope record from Lake E5. **a.** A comparison between
 266 summer (JJA) insolation (Laskar et al., 2004), Lake E5 $\delta D_{\text{precipitation}}$ and inferred
 267 temperature anomalies with 75% and 25% confidence bounds shown for temperature
 268 estimates, relative greenhouse gas radiative forcing from CO_2 , CH_4 , and N_2O (Köhler et
 269 al., 2017), and the NGRIP $\delta^{18}\text{O}$ record (Andersen et al., 2004).

270

271 Leaf wax *n*-acids are present throughout the Lake E5 core, with the sum of *n*- C_{16} -
 272 C_{32} ranging from an average of $59 \mu\text{g g sed}^{-1}$ in the glacial-aged sediments to $1596 \mu\text{g g}$
 273 sed^{-1} in the Holocene sediments (Figure S5). The carbon preference index is 5.8 ± 2.2 ,
 274 while the average chain length averages 25.3 ± 0.8 (Figure S5). Changes in the *n*-acid
 275 distribution between the sedimentary units in Lake E5 support the previous pollen
 276 observations of plant community turnover during the deglacial period. In particular, the
 277 deglacial sediments see an increase in the *n*-acid average chain length, driven by a
 278 reduction in C_{22} and C_{24} *n*-acid and increase in C_{28} and C_{30} *n*-acid, which is consistent
 279 with an expansion of graminoid grasses at that time.

280 The raw n -C₂₈ fatty acid δD_{wax} at Lake E5 ranges from -280 ‰ to -244 ‰ and
281 exhibits distinct glacial-interglacial structure characterized by more negative values
282 during the last glacial period, a peak in the early Holocene, and a declining trend
283 thereafter until the last 150 years (Figure 3). The most pronounced change is a step-
284 increase in δD_{wax} centered at 11.6 ± 0.2 ka, coinciding with the termination of the
285 Younger Dryas stadial. Other Alaska isotope records that span the YD interval, namely
286 $\delta^{18}\text{O}$ of ice wedges (Meyer et al., 2010) and $\delta^{18}\text{O}$ of willow stems (Epstein, 1995;
287 Gaglioti et al., 2017) also show a rapid increase at the termination of the YD (Figure 4).
288 In these records, pre-YD $\delta^{18}\text{O}$ values are comparable to the post-YD values, suggesting
289 the YD was a brief interruption between Bølling and early Holocene warmth as is evident
290 in Greenland ice core $\delta^{18}\text{O}$. In contrast, δD_{wax} values of the Bølling warm period do not
291 achieve post-YD values at Lake E5 and are only slightly D-enriched relative to LGM
292 samples. This difference could result from the water isotope proxies recording different
293 seasons, wherein the Bølling-Allerød warming signal was more pronounced in winter
294 than summer. Given that the willow stems are thought to capture the same seasonality as
295 the leaf waxes, however, it is more likely that a temporary expansion of graminoid sedges
296 during the Bølling-Allerød and late deglacial (Abbott et al., 2010; Eisner and Colinvaux,
297 1992) impacted the record of δD_{wax} , masking a potential BA signal. A slight shift toward
298 longer carbon chain lengths in the n -acid distributions during the graminoid expansion
299 (Figure S5) is further evidence for a vegetation effect. Because Arctic graminoids express
300 stronger D/H fractionation than dicotyledenous shrubs or forbs (Berke et al., 2019;
301 Daniels et al., 2018; Daniels et al., 2017), the observed vegetation change would suppress
302 a change in δD_{wax} during the Bølling interval.

303 The effect of the vegetation-based correction is most notable during the deglacial
304 period, and brings the Bølling- to post-YD differential in better alignment with the
305 Alaska $\delta^{18}\text{O}$ records (Figure 4). It also slightly amplifies glacial-interglacial δD change,
306 as there were more graminoids during the glacial period than the Holocene, and also
307 indicates that changes in $\delta D_{\text{precipitation}}$ likely began prior to the 11.6 ka step change.



308

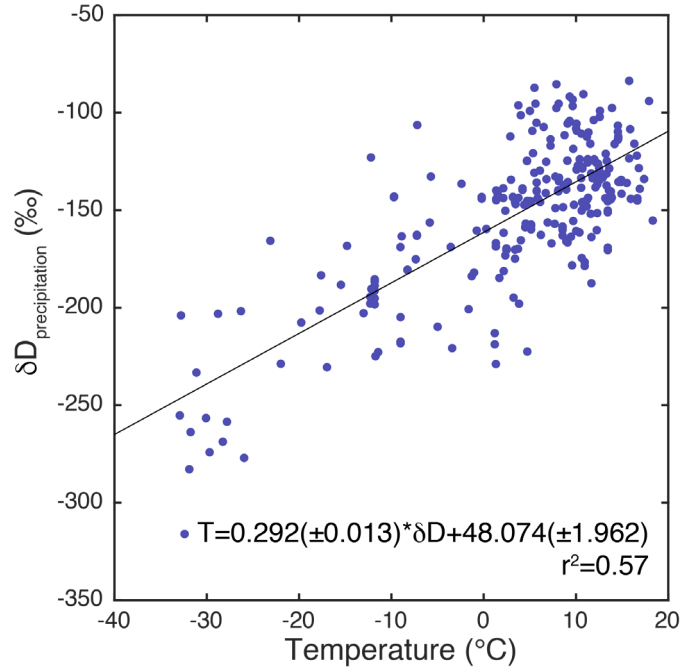
309 **Figure 4.** Comparison of Alaska water isotope records during the Younger Dryas interval
 310 demonstrating that the vegetation-based correction brings the Lake E5 D/H record into
 311 better agreement with other nearby isotope records. a) Ice-volume corrected δD_{wax} from
 312 Lake E5 (black with gray shading showing 1σ of analytical uncertainty), and the inferred
 313 $\delta D_{precipitation}$ following application of the pollen-guided fractionation factors (red with pink
 314 shading showing 25 and 75% confidence intervals of the monte carlo simulation); b) Ice
 315 wedge $\delta^{18}O$ values from Barrow, Alaska (Meyer et al., 2010); c) Salix (willow shrub)
 316 cellulose $\delta^{18}O$ from the North Slope of Alaska (Epstein, 1995; Gaglioti et al., 2017).
 317 Timing of the dual-phase opening of the Bering Strait is also shown (Pico et al., 2020).

318

319 3.2 Modern Precipitation Isotopes

320

A total of 254 precipitation events at the Toolik Field Station were collected and
 321 analyzed, documenting a significant relationship between air temperature and δD (Figure
 322 5). The total least square regression has a slope of $0.292 \text{ ‰ } ^\circ\text{C}^{-1}$, equivalent to $3.4 \text{ } ^\circ\text{C } \text{‰}^{-1}$.
 323 This value is in close agreement with the slope observed in other parts of Arctic North
 324 America (Porter et al., 2016).



325

326 **Figure 5.** Modern relationship between $\delta D_{\text{precipitation}}$ and air temperature at Toolik Lake,
 327 AK based on 254 precipitation events, supported in part by USNIP (US Network for
 328 Isotopes in Precipitation (Welker, 2000; Welker, 2012).

329

330 4. Discussion

331 4.1 Climatic interpretation of $\delta D_{\text{precipitation}}$

332 Due to the strong relationship between air temperature and $\delta D_{\text{precipitation}}$ in the
 333 Arctic (Dansgaard, 1964) and at our site (Figure 5), $\delta D_{\text{precipitation}}$ is a useful proxy for
 334 reconstructing past air temperature (Klein et al., 2015; Pautler et al., 2014; Porter et al.,
 335 2019). Changes in moisture source that resulted from changes in Arctic sea ice cover, site
 336 continentality, or prevailing wind directions could impart effects on $\delta D_{\text{precipitation}}$ at Lake
 337 E5, but we posit that such effects are secondary to the control of condensation
 338 temperature at the site, and that they in fact contribute to the empirical relationship
 339 between temperature and $\delta D_{\text{precipitation}}$ that we observe in modern monitoring. The Arctic
 340 Ocean and the North Pacific are the two dominant sources of moisture to the North Slope of
 341 Alaska. Precipitation originating in the Gulf of Alaska is more D-depleted than Arctic
 342 Ocean or Bering Sea moisture sources because of a larger rainout trajectory and
 343 orographic rainout as airmasses move across the Alaska interior (Lachniet et al., 2016;
 344 Putman et al., 2017). The more negative δD signature of southern airmasses occurs
 345 despite the Arctic Ocean being $\sim 15\%$ D-depleted relative to the North Pacific (Schmidt

346 et al., 1999). A smaller-scale and reversed precipitation isotope gradient is also observed
347 across the North Slope, wherein Arctic moisture becomes D-depleted as it travels
348 southward (Gaglioti et al., 2017). Although these “source effects” are influential,
349 seasonal changes in moisture source are largely controlled by sea ice coverage, which
350 together with air temperature, gives rise to a strong seasonal cycle in $\delta D_{\text{precipitation}}$ at Lake
351 E5 (Daniels et al., 2017) and a positive correlation between air temperature and
352 $\delta D_{\text{precipitation}}$. Because these seasonal changes are analogous to changes over glacial-
353 interglacial time scales, the modern temperature- $\delta D_{\text{precipitation}}$ relationship offers a transfer
354 function for approximating past temperature in northern Alaska.

355 The utility of the modern temperature- $\delta D_{\text{precipitation}}$ relationship is further
356 supported by an investigation of isotope-enabled climate model simulations of the past 20
357 ka which shows that the relationship between temperature and $\delta D_{\text{precipitation}}$ has remained
358 approximately constant since the LGM (Figure S6). The modeled modern slope is
359 substantially lower than the observed relationship between temperature and $\delta D_{\text{precipitation}}$,
360 but the modeled slopes remains stable during and since the LGM, reflecting the
361 approximate stationarity of the temperature- $\delta D_{\text{precipitation}}$ relationship over this interval.
362 Temperature anomalies are calculated using the observed modern slope of $3.4 \text{ ‰ } ^\circ\text{C}^{-1}$,
363 which is similar to the slope reported across a number of Arctic North American sites
364 ($3.1 \text{ ‰ per } ^\circ\text{C}$ Porter et al., 2016).

365 Estimates of temperature change from δD_{wax} are also influenced by the
366 seasonality of precipitation used for plant leaf wax synthesis. Although tundra plant
367 growth is constrained to the summer growing season, the water used in their biosynthesis
368 has been linked to both warm and cold season precipitation sources (Jespersen et al.,
369 2018; Welker et al., 2005). Wilkie et al. (2012) suggest a bias toward use of remnant
370 autumnal precipitation in supporting spring leaf production, whereas others have used
371 terrestrial wax D/H as a proxy for summer precipitation (Porter et al., 2016; Thomas et
372 al., 2012). In our study area, approximately 60% of the annual precipitation falls during
373 JJA (Cherry et al., 2014); Daniels et al. (2017) identify seasonally changing soilwater
374 isotopic composition throughout the growing season, and suggest that although cold
375 season precipitation can contribute to biosynthesis, summer rainfall is the most important
376 hydrogen source for leaf wax production. Given the mixture of seasonal precipitation

377 utilized by tundra plants, the potential for changing growing season lengths, and the
378 strong event-based correlation between temperature and $\delta D_{\text{precipitation}}$ across the seasons,
379 we use the annual temperature- $\square D_{\text{precipitation}}$ relationship to translate our δD_{wax}
380 measurements into summer-biased temperature change estimates.

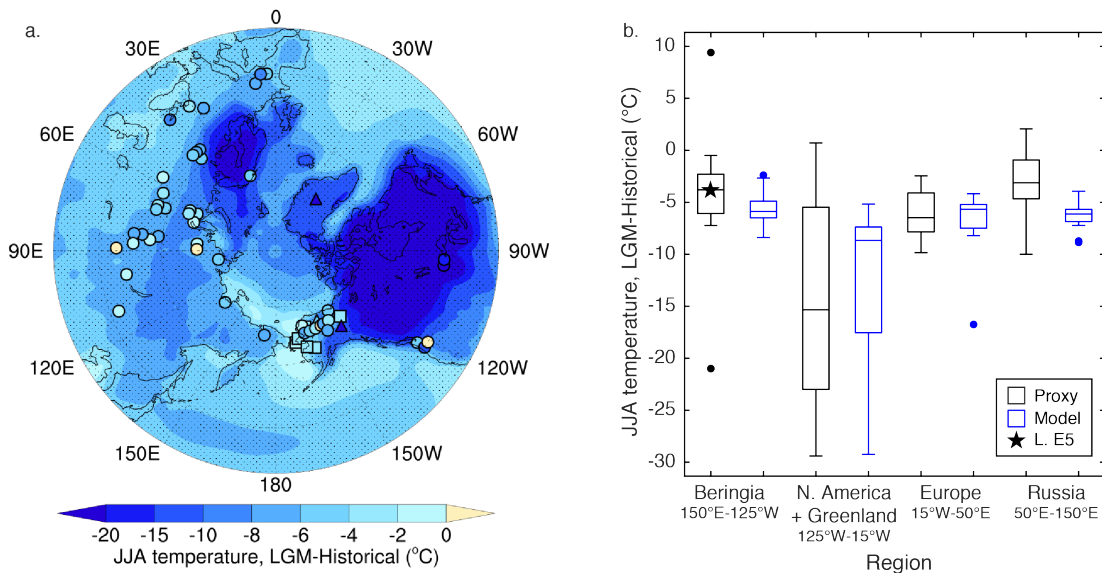
381

382 4.2 Glacial-Interglacial Climate Change

383 The vegetation-corrected $\delta D_{\text{precipitation}}$ and inferred temperatures at Lake E5 exhibit
384 distinct glacial-interglacial structure (Figure 3) with inferred temperatures during the
385 LGM 3.7 ± 1.8 °C lower than during the Historical Period (1900-2014 CE) and just 2.9
386 °C lower than during the Pre-industrial period (PI; 2-0.1 ka). The estimated ΔT of -3.7°C
387 for the LGM is less severe than LGM cooling observed in Greenland, northern Europe,
388 and other parts of North America (Figure 6), but is within the range of previous estimates
389 for Eastern Beringia (Table S4, and references therein). These mild conditions were
390 likely important for maintaining the highly-productive mammoth-steppe tundra (Zimov et
391 al., 2012) and sustaining human occupation of Beringia through the LGM (Goebel et al.,
392 2008; Vachula et al., 2019).

393 We examined the ensemble output from the Paleoclimate-Model Intercomparison
394 Project 3 (PMIP3) and find significant spatial variability in LGM temperature change
395 across the Arctic (Figure 5). The model results agree well with proxy reconstructions and
396 indicate LGM cooling was weaker in Beringia than other Arctic regions. These results
397 could support the hypothesis that orographic steering of atmospheric heat by the LIS
398 mitigated LGM cooling in Alaska (Bartlein et al., 2011; Briner and Kaufman, 2008; Otto-
399 Bliesner et al., 2006). In the simulations, mild LGM temperatures are localized over the
400 Bering Strait. This implies that exposure of the Bering Land Bridge, through its effects on
401 surface energy balance (Bartlein et al., 2015), was an important driver of mild LGM
402 temperatures in the Bering Strait vicinity. West of the Bering Strait, moderating effects of
403 the ice-sheet orography and land-bridge were less pronounced, with LGM summer
404 temperatures at Lake El'gygytgyn in Far East Russia 8-9 °C colder than present (Melles
405 et al., 2012), nearly double the global average of 4.9 °C (Shakun and Carlson, 2010).
406 Likewise, to the southeast of our site, in central Yukon Territory and in close proximity
407 to the Laurentide and Cordilleran Ice Sheets, Porter et al. (2016) report that LGM

408 temperatures were 14-21 °C below present day. Thus, while much of North America,
 409 Europe, and Asia experienced enhanced LGM cooling due to continental ice sheet and
 410 sea ice growth and possible redirection of polar air masses into those regions (Miller et
 411 al., 2010), Beringia-specific changes in land exposure and the advection of relatively
 412 warm air dampened LGM cooling, resulting in regionally distinct expressions of Arctic
 413 Amplification.
 414



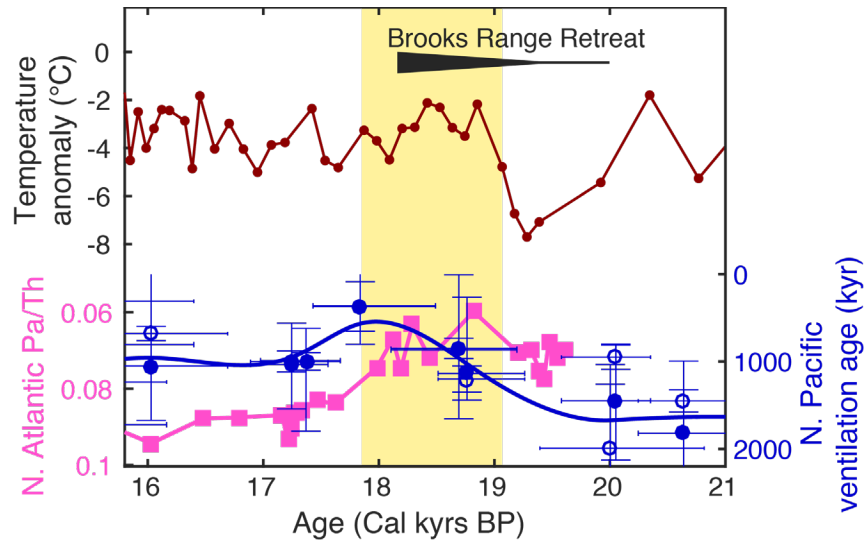
415
 416 **Figure 6.** Data-model comparison of LGM warm-season temperature anomalies across
 417 the Arctic. **a.** PMIP3 multi-model ensemble average JJA temperature anomalies relative
 418 to the historical period (1900-2000 CE) overlain by published LGM temperature
 419 reconstructions based on pollen (circles), insects (squares), and geochemistry (triangles)
 420 (Table S4). **b.** LGM temperature anomalies in proxies and the multi-model means in four
 421 sectors of the Arctic. Model data are extracted from gridcells within 2° of proxy sites, and
 422 do not include ice-sheet or ocean cells, with the exceptions of the Greenland and Norway
 423 locations, for which ice-free grid cells are not available in models.
 424

425 4.3 Rapid Changes During the Glacial Termination

426 δD_{wax} at Lake E5 generally tracks changes in summer insolation, with warming
 427 evident as early as 23.1 ± 0.9 ka. Steady, more substantial deglacial warming began at
 428 16.9 ± 0.5 ka, coinciding with increased radiative forcing from greenhouse gases (Köhler
 429 et al., 2017), and culminating in a brief period of rapid temperature rise at 14.8 ± 0.3 ka.
 430 Temperatures rose by 8.4 ± 0.5 °C from the LGM to an early Holocene thermal maximum
 431 (HTM) from 11.6-9.5 ka, then cooled steadily until the PI era. While the overall

432 correspondences between temperature, greenhouse gas forcing, and summer insolation
433 are strong, we observe several intervals of abrupt warming and cooling during the glacial
434 termination (Figure 3).

435 Early in the glacial termination, there was rapid warming of ~ 5 °C in Arctic
436 Alaska from 19.3 ± 0.7 ka to 18.9 ± 0.7 ka. This warming can help explain suggestions of
437 rapid glacier retreat in the nearby Brooks Range mountains dated to 19 ka (Pendleton et
438 al., 2015). The causes for this early, strong warming have been enigmatic, and include
439 increasing summer insolation and a maximum in the effect of the LIS on atmospheric
440 flow (Pendleton et al., 2015), but it is unclear how these processes would produce the
441 abrupt, short-lived warming observed in the δD_{wax} record. We propose an oceanic driver
442 of this warming event. Ventilation ages of the North Pacific document an invigorated
443 PMOC beginning at 19 ka (Figure 7) which would have increased the total northward
444 heat transport in the Pacific by approximately 0.7 PW, with the greatest amount of
445 resultant ocean warming near the Gulf of Alaska and Bering Strait (Okazaki et al., 2010).
446 Model simulations indicate that PMOC intensifies in response to AMOC collapse (Hu et
447 al., 2012), for example during HS1, due to reduced evaporation and increased sea surface
448 salinity in the North Pacific. We note, however, that empirical evidence for PMOC
449 intensification predates the reduction in AMOC marking the onset of HS1 (Figure 2c;
450 McManus et al., 2004; Okazaki et al., 2010). While the cause of this PMOC
451 invigoration remains uncertain, the increased northward oceanic heat transport in both
452 oceans likely contributed to warming from 19-18 ka in Alaska, while subsequent HS1
453 cooling may have been suppressed in Alaska by sustained PMOC activity.



454

455 **Figure 7.** Comparison of early deglacial warming at Lake E5 and marine indicators of
 456 PMOC and AMOC intensity. Temperature anomaly (red) is based on δD_{wax} relative to the
 457 historical period. N. Pacific ventilation ages (blue) reflect PMOC intensity (Okazaki et
 458 al., 2010), while Pa/Th from the Bermuda Rise (magenta) is an indicator of AMOC
 459 intensity (McManus et al., 2004). Also shown is the period of rapid glacier retreat in the
 460 Brooks Range mountains near Lake E5 (Pendleton et al., 2015).
 461

462 Abrupt warming at 14.8 ± 0.3 and 11.6 ± 0.2 ka in the Lake E5 record (Figure 3)
 463 correspond with the onset of the Bølling interstadial and the termination of the Younger
 464 Dryas, indicating Arctic Alaskan temperature change was positively correlated with
 465 changes in the North Atlantic during the latter part of the deglaciation. Temperatures
 466 warmed by ~ 5 °C at the Bølling onset and ~ 4 °C over the YD termination, much smaller
 467 than the 9 °C changes reconstructed over Greenland (Severinghaus and Brook, 1999).
 468 Both events are driven by strengthening and possible “overshoot” of AMOC (Liu et al.,
 469 2009). While BA-YD fluctuations are seen in oceanographic records of the Bering Sea
 470 (Kühn et al., 2014) and Gulf of Alaska (Praetorius and Mix, 2014), the much larger
 471 surface warming observed at Greenland indicates that the surface temperature response to
 472 AMOC variability is weaker in continental Beringia. Furthermore, comparison of the
 473 Lake E5 $\delta D_{precipitation}$, which records summer variability, with ice wedge isotopes in
 474 Barrow, AK, which record winter conditions, suggests that the BA-YD oscillation was
 475 expressed most strongly in the winter season. Nevertheless, the two events encompass
 476 most of the deglacial temperature increase at Lake E5. The Bølling-onset inferred here
 477 slightly precedes a vegetation shift from herb steppe tundra to deciduous shrub tundra

478 between 13.9 and 12.6 seen in Brooks Range-area pollen records (Abbott et al., 2010;
479 Mann et al., 2002; Oswald et al., 1999). The timing offset between increased δD_{wax} and
480 the rise of shrub tundra may result from limits of the age models, or indicate that the
481 isotopic proxy responds faster to climatic change than do vegetation assemblages. The
482 expansion of shrubs would have accelerated deglacial warming by increasing the surface
483 energy balance of the Alaska land surface by 2-3 W m^{-2} (Lynch et al., 1999), similar to
484 changes occurring today (Elmendorf et al., 2012; Sturm et al., 2001).

485 The pre-YD warm interval occurred in two phases, interrupted by a short-lived
486 cool period at approximately 14 ka correlating with the Older Dryas interval recognized
487 from the North Atlantic (Grootes and Stuiver, 1997; Mangerud et al., 2017) region as
488 well as the North Pacific (Kienast and McKay, 2001). Following this, temperatures
489 increased by 2-4 $^{\circ}\text{C}$ between 13.5 ± 0.3 and 12.8 ± 0.2 ka, marking the onset of a warm
490 interval correlating with the Allerød Interstadial. In contrast to the NGRIP isotope record
491 which suggests cooling across the B-A (Andersen et al., 2004) the Bølling and Allerød
492 periods are of comparable temperatures at Lake E5. This contrast is also recognized in
493 Southern Alaska (Hu et al., 2006), and could arise from processes local to Beringia, such
494 as the flooding of the Bering Land Bridge, which possibly enhanced Allerød warming in
495 the area.

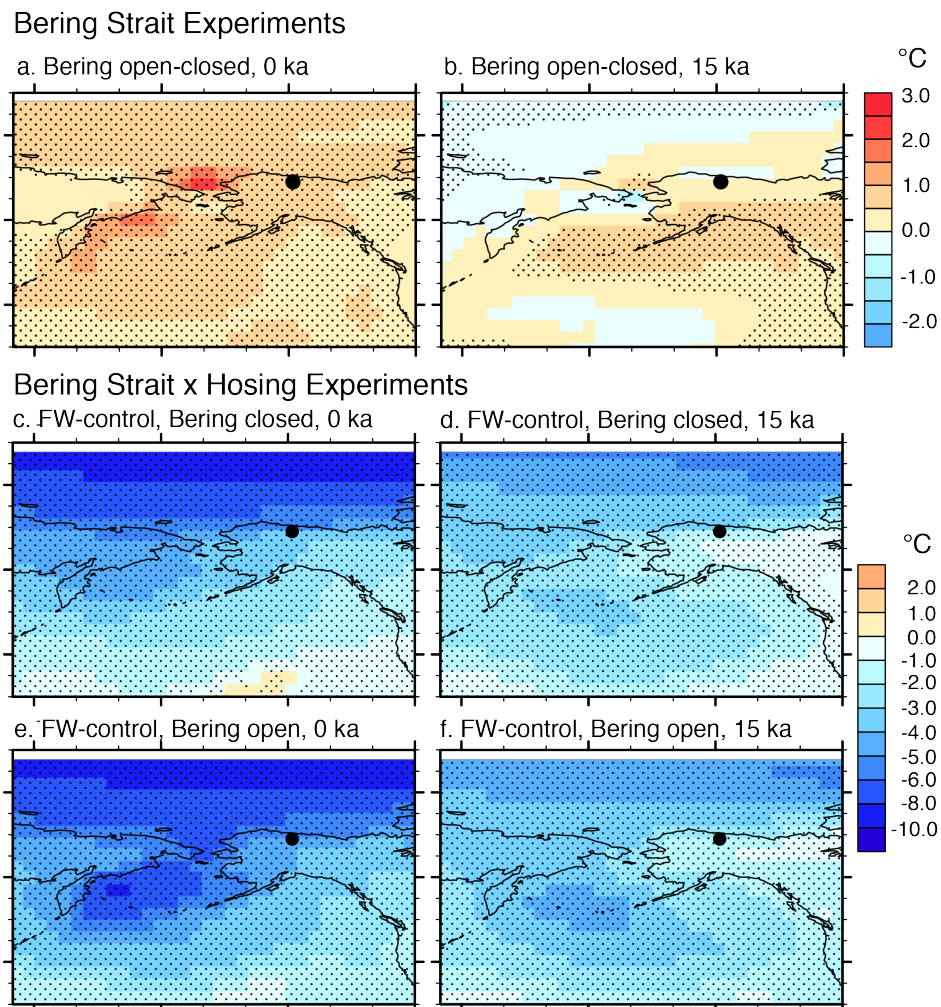
496 The submergence of the Bering land bridge during the late deglacial likely had
497 profound impact on Beringia climate (Bartlein et al., 2015). The Pacific and Arctic
498 Oceans became connected between 11 and 13.4 ka (England and Furze, 2008; Jakobsson
499 et al., 2017), although the timing is not precisely known (Clark et al., 2014). Geophysical
500 modeling of regional ice sheets and isostatic adjustment suggests the possibility of a two-
501 phase land bridge inundation, with the first Pacific-Arctic connection forming ~ 13.3 ka,
502 followed by a more substantive flooding event ~ 11.5 ka, with these periods bracketing an
503 approximate intermission in local sea level change (Pico et al., 2020). Their model
504 identifies regional isostatic rebound from 13 to 11.5 ka, driven by mass loss from the
505 Cordilleran and western Laurentide Ice Sheet, as the principal driver of the hiatus in
506 Bering Strait flooding. If the warming signal at 13.4 ka in the Lake E5 δD_{wax} record
507 represents a regional warming event, this may have provided an important mechanism
508 contributing to retreat of ice sheets at that time.

509 We tested the impacts of Bering submergence using idealized experiments in
510 CCSM3 by simulating Beringia surface temperatures under Bering Strait open and closed
511 scenarios (BSO and BSC) and under 15 ka (deglacial) and 0 ka (interglacial) climate
512 boundary conditions. Upon opening of the strait we observe little change, or cooling in
513 the annual temperature immediately over the Bering Sea, similar to findings from
514 Bartlein et al. (2015). However, moving away from the strait, the effect is reversed, with
515 0.5-1.5 °C warming over interior Alaska (Figure 8). The effect is stronger warming under
516 interglacial climate conditions. Thus, although the simulations are idealized and do not
517 test the climate impacts of initial strait opening, they provide qualitative support for the
518 idea that increased Bering Strait throughflow warms interior Alaska, despite the fact that
519 the marine transgression resulted in summer cooling in the immediate vicinity of the
520 Bering Strait. An early opening of the Bering Strait (~13.3 ka) may therefore be linked to
521 enhanced Allerød warming, whereas a late opening (~11.5 ka) may have contributed to
522 YD-termination warmth and a sustained early Holocene warm period in Eastern Beringia.
523 Surface albedo feedbacks associated with expansion of forest and shrubs into the steppe
524 tundra as well as the establishment of ice-free ocean during summers may have also
525 contributed to a relatively warm Allerød interval.

526 Abrupt warming events at 13.5 ka and 11.6 ka bracket a Younger Dryas cool
527 interval. Across Eastern Beringia, indications of YD climate anomalies variably are
528 absent (Kokorowski et al., 2008; Kurek et al., 2009a; Kurek et al., 2009b), demonstrate
529 wintertime cooling (Meyer et al., 2010), demonstrate summertime cooling (Engstrom et
530 al., 1990; Gaglioti et al., 2017; Hamilton, 2003; Mann et al., 2010), or suggest a return to
531 arid conditions (Abbott et al., 2000; Mann et al., 2002). In Lake E5, δD_{wax} decreased by
532 10 ‰ beginning at 12.8 ± 0.2 ka, equivalent to approximately 3 °C of summer cooling.

533 The YD climate reversal is typically attributed to surface water freshening in the
534 North Atlantic, slowing of AMOC, and reduction of northward oceanic heat transport
535 into the high northern latitudes. We tested the impacts of these processes on Beringian
536 climate using idealized freshwater hosing experiments in the CCSM3 by simulating
537 AMOC collapse under the same scenarios as the Bering Strait experiments (Figure 8).
538 Under deglacial boundary conditions, AMOC collapse results in a range of cooling of 1-3
539 °C in Alaska for a fully-open strait and 0-2 °C when the strait is already closed. Under

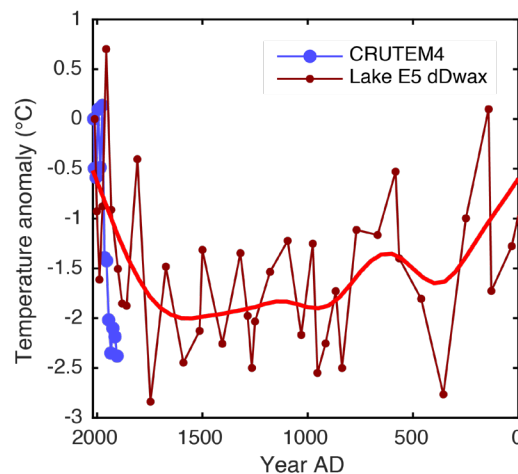
540 present-day (0 ka) boundary conditions, the temperature sensitivity to North Atlantic
 541 freshwater forcing is approximately double that of the deglacial simulations for both BSO
 542 and BSC scenarios, suggesting that a weakened AMOC has a much larger impact on
 543 Arctic Alaskan climate when the global climate is warmer. In addition, the prediction that
 544 the magnitude of cooling is ~50% weaker when the Bering Strait is closed, may help
 545 explain the weak expression of HS1 in Lake E5 sediments.
 546



547
 548 **Figure 8:** Mean annual surface temperature anomalies in Beringia in CCSM3
 549 experiments. Stippling represents anomalies that are statistically significant at the $p =$
 550 0.05 level according to a t-test. **a.** and **b.** Mean annual temperature anomalies between
 551 simulations with open and closed Bering Strait under present-day (1990 A.D.) and 15 ka
 552 boundary conditions, respectively; **c.** and **d.** Mean annual temperature anomaly between
 553 hosing experiments and control simulations under closed Bering Strait conditions for 0 ka
 554 and 15 ka; **e.** and **f.** Same as **c.** and **d.** but with an open Bering Strait.
 555

556 3.4 Climate of the Holocene

557 The most prominent feature of the Holocene is a $\delta D_{\text{precipitation}}$ and inferred-
558 temperature maximum from ~ 11.6 to 9.5 ka (Figure 3), followed by a gradual cooling
559 until the PI period. Temperature during this Holocene Thermal Maximum (HTM)
560 averaged 5.5 ± 1.7 °C warmer than during the PI (19 ‰), and 4.7 ± 1.7 °C warmer than
561 the Historical Period (16 ‰). The timing of the HTM is approximately synchronous with
562 peak NH summer insolation (Figure 3), thus occurring slightly earlier than in the Yukon
563 Territory (Porter et al., 2019) and locations further east (Kaufman, 2004). The
564 termination of the HTM occurs abruptly, with ~ 2 °C of cooling at 9.5 ± 0.2 ka, followed
565 by gradual cooling that follows trends in summer insolation. Analogous declines in
566 lacustrine $\delta^{18}\text{O}$ proxies are recorded at nearby Schrader Pond in Northeast Alaska
567 (Broadman et al., 2020), as well as a number of sites in southern and central Alaska
568 (Anderson et al., 2001; Vachula et al., 2017). These records, which together document
569 cooling and drying of Beringia climate over the Holocene, with a particular bias towards
570 summer conditions, contrast with the Lake E5 alkenone record which is proposed to
571 record a wintertime warming signal over the Holocene in response to increasing cold-
572 season insolation (Longo et al., 2020). After brief warm periods at $\sim 5.6 \pm 0.2$ ka and from
573 4.0 to 3.5 ka, re-intensified cooling from 4 to 0.1 ka is synchronous with the expansion of
574 alpine glaciers in the Brooks Range (Badding et al., 2013). Temperatures were more
575 stable during the PI interval, but still cooled at a rate of ~ 0.5 °C per millennium,
576 exceeding the average pan-Arctic late Holocene cooling of 0.22 °C per thousand years
577 (Kaufman et al., 2009).



578

579 **Figure 9.** Lake E5 δD_{wax} -inferred temperature anomalies over the past 1000 years (red,
580 with smoothing spline) and CRUTEM4 instrumental observations from Northern Alaska
581 (blue).
582

583 The Lake E5 $\delta D_{\text{precipitation}}$ record contextualizes ongoing Alaska warming in the
584 prism of climate changes of the past ~ 32 kyr. Modern (coretop) leaf waxes from the
585 historical era at Lake E5 are D-enriched relative to the PI average by 5.2 ± 0.8 ‰,
586 equating to 1.7 ± 0.6 °C of warming (Figure 9). The amplitude of warming we
587 reconstruct at Lake E5 is slightly smaller than both the 2.5°C of JJA warming apparent in
588 the CRUTEM4 instrumental database for Northern Alaska (Jones et al., 2012) and the
589 2°C rise in mean annual temperature inferred from the nearby McCall glacier ice core
590 $^{18}\text{O}/^{16}\text{O}$ ratios (Klein et al., 2015). Furthermore, whereas, Porter et al. (2019) show, based
591 on $^{18}\text{O}/^{16}\text{O}$ in ground ice, that recent warming in Central Yukon has surpassed peak early-
592 Holocene warmth, this is not the case at Lake E5. Likewise, $\delta^{18}\text{O}$ values in diatoms at
593 nearby Schrader Lake decline during the Holocene but do not exhibit the a reversal to
594 HTM levels (Broadman et al., 2020). Nonetheless, the isotope-inferred warming at Lake
595 E5, in conjunction with the instrumental observations, indicate that recent temperature
596 increase in northern Alaska exceeds the +1.4 °C pan-Arctic temperature change between
597 the pre-industrial period and today (Kaufman et al., 2009). This amplified warming
598 contrasts with the spatial pattern of temperature change across the deglaciation, when
599 Beringian warming was smaller than other parts of the Arctic. The contraction of winter
600 and summer sea ice in the adjacent Chukchi Sea (Serreze et al., 2007; Stroeve et al.,
601 2012) and the expansion of shrubs into low tundra biomes (Elmendorf et al., 2012; Sturm
602 et al., 2001) are likely feedbacks amplifying recent warming in northern Alaska.

603

604 **5. Conclusions**

605 A new record of Eastern Beringia paleoclimate provides evidence for a relatively
606 mild LGM and a series of abrupt climate transitions during the deglacial period, with
607 rapid warming observed at 19 ka, 14.8 ka, 13.4 and 11.6 ka, during which temperature
608 increased by 4-5 °C in under 300 years. Furthermore, data-model comparisons
609 demonstrate that the magnitude of paleo-arctic amplification in this region has evolved
610 from the last glacial period to today. In particular, whereas muted LGM cooling in

611 Beringia indicates strong ameliorating effects of ice sheet orography and possibly
612 enhanced continentality, the Holocene and modern changes are amplified relative to other
613 Arctic sites, which we speculate is due to surface feedbacks including recent sea ice
614 decline and shrub expansion in conjunction with the removal of factors such as the LIS
615 which dampened regional temperature change during the deglacial. Model results suggest
616 greater climate sensitivity to North Atlantic freshwater forcing under modern-day, open
617 Bering-Strait conditions, than under late-glacial conditions. These results predict that
618 Arctic Alaskan temperatures will continue to warm more rapidly in the future than other
619 sectors of the Arctic.

620

621 **Acknowledgments**

622 This work is partially supported by National Geographic grant 9397-13 (Y.H.),
623 and National Science Foundation grants PLR-1503846 (Y.H., J.M.R.), PLR-1504069
624 (C.M.) and DEB-1026843 (ARC-LTER), and 0923571 (J.M.W.) and a National Ocean
625 Sciences Accelerator Mass Spectroscopy Graduate Student Internship (W.M.L.). A.H. is
626 supported by the Regional and Global Model Analysis (RGMA) component of the Earth
627 and Environmental System Modeling Program of the U.S. Department of Energy's Office
628 of Biological & Environmental Research Cooperative Agreement # DE-FC02-
629 97ER62402, and the NSF. The National Center for Atmospheric Research is sponsored
630 by the NSF. This research used resources of the National Energy Research Scientific
631 Computing Center, a DOE Office of Science User Facility supported by the Office of
632 Science of the DOE under Contract No. DE-AC02-05CH11231. We thank Rafael Tarozo
633 for laboratory assistance.

634

635 **Data availability**

636 Lake E5 leaf wax hydrogen isotope data and precipitation isotope data from the
637 Toolik Field Station are freely available at the Arctic Data Center Archives. Upon
638 publication, the sediment record will be archived at the NOAA paleoclimate database,
639 and this statement will be updated with a DOI accordingly.

640

641 **Competing Interests**

642 The authors declare no competing interests.

643

644 **References**

645 Abbott, M.B., Edwards, M.E., Finney, B.P., 2010. A 40,000-yr record of environmental
646 change from Burial Lake in Northwest Alaska. *Quatern. Res.* 74, 156-165.

647 Abbott, M.B., Finney, B.P., Edwards, M.E., Kelts, K.R., 2000. Lake-level reconstruction
648 and paleohydrology of Birch Lake, central Alaska, based on seismic reflection profiles
649 and core transects. *Quatern. Res.* 53, 154-166.

650 Andersen, K.K., Azuma, N., Barnola, J.-M., Bigler, M., Biscaye, P., Caillon, N.,
651 Chappellaz, J., Clausen, H.B., Dahl-Jensen, D., Fischer, H., 2004. High-resolution record
652 of Northern Hemisphere climate extending into the last interglacial period. *Nature* 431,
653 147-151.

654 Anderson, L., Abbott, M.B., Finney, B.P., 2001. Holocene climate inferred from oxygen
655 isotope ratios in lake sediments, central Brooks Range, Alaska. *Quatern. Res.* 55, 313-
656 321.

657 Badding, M.E., Briner, J.P., Kaufman, D.S., 2013. ^{10}Be ages of late Pleistocene
658 deglaciation and Neoglaciation in the north - central Brooks Range, Arctic Alaska.
659 *Journal of Quaternary Science* 28, 95-102.

660 Bartlein, P., Edwards, M., Hostetler, S., Shafer, S., Anderson, P., Brubaker, L., Lozhkin,
661 A., 2015. Early-Holocene warming in Beringia and its mediation by sea-level and
662 vegetation changes. *Climate of the Past Discussions* 11, 873-932.

663 Bartlein, P., Harrison, S., Brewer, S., Connor, S., Davis, B., Gajewski, K., Guiot, J.,
664 Harrison-Prentice, T., Henderson, A., Peyron, O., 2011. Pollen-based continental climate
665 reconstructions at 6 and 21 ka: a global synthesis. *Climate dynamics* 37, 775-802.

666 Berke, M.A., Sierra, A.C., Bush, R., Cheah, D., O'Connor, K., 2019. Controls on leaf
667 wax fractionation and $\delta^2\text{H}$ values in tundra vascular plants from western Greenland.
668 *Geochim. Cosmochim. Acta* 244, 565-583.

669 Blaauw, M., 2010. Methods and code for 'classical' age-modelling of radiocarbon
670 sequences. *quaternary geochronology* 5, 512-518.

- 671 Briner, J.P., Kaufman, D.S., 2008. Late Pleistocene mountain glaciation in Alaska: key
672 chronologies. *Journal of Quaternary Science* 23, 659-670.
- 673 Broadman, E., Kaufman, D.S., Henderson, A.C., Malmierca-Vallet, I., Leng, M.J., Lacey,
674 J.H., 2020. Coupled impacts of sea ice variability and North Pacific atmospheric
675 circulation on Holocene hydroclimate in Arctic Alaska. *Proceedings of the National
676 Academy of Sciences* 117, 33034-33042.
- 677 Broccoli, A.J., Manabe, S., 1987. The effects of the Laurentide ice sheet on North
678 American climate during the last glacial maximum. *Geographie physique et Quaternaire*
679 41, 9.
- 680 Broecker, W.S., Kennett, J.P., Flower, B.P., Teller, J.T., Trumbore, S., Bonani, G.,
681 Wolfli, W., 1989. Routing of meltwater from the Laurentide Ice Sheet during the
682 Younger Dryas cold episode.
- 683 Cherry, J.E., Déry, S.J., Stieglitz, M., Pan, F.-f., 2014. Meteorology and climate of Toolik
684 Lake and the north slope of Alaska: Past, present and future. *Alaska's changing Arctic:
685 Ecological consequences for tundra, streams, and lakes*. Oxford Univ. Press.
- 686 Chikaraishi, Y., Naraoka, H., 2007. $\delta^{13}\text{C}$ and δD relationships among three n-alkyl
687 compound classes (n-alkanoic acid, n-alkane and n-alkanol) of terrestrial higher plants.
688 *Org. Geochem.* 38, 198-215.
- 689 Clark, J., Mitrovica, J.X., Alder, J., 2014. Coastal paleogeography of the California–
690 Oregon–Washington and Bering Sea continental shelves during the latest Pleistocene and
691 Holocene: implications for the archaeological record. *Journal of Archaeological Science*
692 52, 12-23.
- 693 Dahl-Jensen, D., Mosegaard, K., Gundestrup, N., Clow, G.D., Johnsen, S.J., Hansen,
694 A.W., Balling, N., 1998. Past temperatures directly from the Greenland ice sheet. *Science*
695 282, 268-271.
- 696 Daniels, W.C., Huang, Y., Russell, J.M., Giblin, A.E., 2018. Effect of continuous light on
697 leaf wax isotope ratios in *Betula nana* and *Eriophorum vaginatum*: Implications for Arctic
698 paleoclimate reconstructions. *Org. Geochem.* 125, 70-81.

- 699 Daniels, W.C., Kling, G.W., Giblin, A.E., 2015. Benthic community metabolism in deep
700 and shallow Arctic lakes during 13 years of whole-lake fertilization. *Limnol. Oceanogr.*,
701 n/a-n/a.
- 702 Daniels, W.C., Russell, J.M., Giblin, A.E., Welker, J.M., Klein, E.S., Huang, Y., 2017.
703 Hydrogen isotope fractionation in leaf waxes in the Alaskan Arctic tundra. *Geochim.*
704 *Cosmochim. Acta* 213, 216-236.
- 705 Dansgaard, W., 1964. Stable isotopes in precipitation. *Tellus* 16, 436-468.
- 706 Dyke, A.S., 2004. An outline of North American deglaciation with emphasis on central
707 and northern Canada. *Quaternary glaciations: Extent and chronology* 2, 373-424.
- 708 Eisner, W.R., Colinvaux, P.A., 1992. Late Quaternary Pollen Records from Oil Lake and
709 Feniak Lake, Alaska, U.S.A. *Arct. Alp. Res.* 24, 56-63.
- 710 Elmendorf, S.C., Henry, G.H., Hollister, R.D., Björk, R.G., Boulanger-Lapointe, N.,
711 Cooper, E.J., Cornelissen, J.H., Day, T.A., Dorrepaal, E., Elumeeva, T.G., 2012. Plot-
712 scale evidence of tundra vegetation change and links to recent summer warming. *Nature*
713 *Climate Change* 2, 453.
- 714 England, J.H., Furze, M.F., 2008. New evidence from the western Canadian Arctic
715 Archipelago for the resubmergence of Bering Strait. *Quatern. Res.* 70, 60-67.
- 716 Engstrom, D., Hansen, B., Wright, H., 1990. A possible Younger Dryas record in
717 southeastern Alaska. *Science* 250, 1383-1385.
- 718 Epstein, S., 1995. The isotopic climatic records in the Alleröd-Bølling-Younger Dryas
719 and Post-Younger Dryas events. *Global Biogeochem. Cycles* 9, 557-563.
- 720 Feakins, S.J., 2013. Pollen-corrected leaf wax D/H reconstructions of northeast African
721 hydrological changes during the late Miocene. *Palaeogeogr., Palaeoclimatol., Palaeoecol.*
722 374, 62-71.
- 723 Gaglioti, B.V., Mann, D.H., Wooller, M.J., Jones, B.M., Wiles, G.C., Groves, P., Kunz,
724 M.L., Baughman, C.A., Reanier, R.E., 2017. Younger-Dryas cooling and sea-ice
725 feedbacks were prominent features of the Pleistocene-Holocene transition in Arctic
726 Alaska. *Quaternary Science Reviews* 169, 330-343.

- 727 Gao, L., Edwards, E.J., Zeng, Y., Huang, Y., 2014. Major Evolutionary Trends in
728 Hydrogen Isotope Fractionation of Vascular Plant Leaf Waxes. PLoS ONE 9, e112610.
- 729 Goebel, T., Waters, M.R., O'rourke, D.H., 2008. The late Pleistocene dispersal of modern
730 humans in the Americas. *science* 319, 1497-1502.
- 731 Graf, K.E., Bigelow, N.H., 2011. Human response to climate during the Younger Dryas
732 chronozone in central Alaska. *Quaternary International* 242, 434-451.
- 733 Grootes, P., Stuiver, M., 1997. Oxygen 18/16 variability in Greenland snow and ice with
734 10⁻³ - to 10⁵ - year time resolution. *Journal of Geophysical Research: Oceans* (1978–
735 2012) 102, 26455-26470.
- 736 Grootes, P., Stuiver, M., White, J., Johnson, S., Jouzel, J., 1993. Comparison of oxygen
737 isotope records from the GISP2 and GRIP Greenland ice cores. *Nature* 366, 3.
- 738 Hamilton, T.D., 2003. Glacial Geology of the Toolik Lake and Upper Kuparuk River
739 Regions, in: Walker, D. (Ed.), *Biological Papers of the University of Alaska*. Institute of
740 Arctic Biology, Fairbanks, Alaska.
- 741 Hu, A., Meehl, G.A., Han, W., Abe - Ouchi, A., Morrill, C., Okazaki, Y., Chikamoto,
742 M.O., 2012. The Pacific - Atlantic seesaw and the Bering Strait. *Geophys. Res. Lett.* 39.
- 743 Hu, A., Meehl, G.A., Han, W., Otto-Blietner, B., Abe-Ouchi, A., Rosenbloom, N., 2015.
744 Effects of the Bering Strait closure on AMOC and global climate under different
745 background climates. *Prog. Oceanogr.* 132, 174-196.
- 746 Hu, F.S., Nelson, D.M., Clarke, G.H., Rühland, K.M., Huang, Y., Kaufman, D.S., Smol,
747 J.P., 2006. Abrupt climatic events during the last glacial - interglacial transition in
748 Alaska. *Geophys. Res. Lett.* 33.
- 749 Jakobsson, M., Pearce, C., Cronin, T.M., Backman, J., Anderson, L.G., Barrientos, N.,
750 Björk, G., Coxall, H., De Boer, A., Mayer, L.A., 2017. Post-glacial flooding of the
751 Bering Land Bridge dated to 11 cal ka BP based on new geophysical and sediment
752 records. *Climate of the Past* 13, 991.

- 753 Jespersen, R.G., Leffler, A.J., Oberbauer, S.F., Welker, J.M., 2018. Arctic plant
754 ecophysiology and water source utilization in response to altered snow: isotopic ($\delta^{18}\text{O}$
755 and $\delta^2\text{H}$) evidence for meltwater subsidies to deciduous shrubs. *Oecologia* 187, 1009-
756 1023.
- 757 Johnsen, S.J., Clausen, H.B., Dansgaard, W., Fuhrer, K., Gundestrup, N., Hammer, C.U.,
758 Iversen, P., Jouzel, J., Stauffer, B., Steffensen, J.P., 1992. Irregular glacial interstadials
759 recorded in a new Greenland ice core. *Nature* 359, 3.
- 760 Jones, M.C., Yu, Z., 2010. Rapid deglacial and early Holocene expansion of peatlands in
761 Alaska. *Proceedings of the National Academy of Sciences* 107, 7347-7352.
- 762 Jones, P.D., Lister, D.H., Osborn, T.J., Harpham, C., Salmon, M., Morice, C.P., 2012.
763 Hemispheric and large-scale land-surface air temperature variations: An extensive
764 revision and an update to 2010. *Journal of Geophysical Research: Atmospheres* 117, n/a-
765 n/a.
- 766 Kaufman, D., 2004. Holocene thermal maximum in the western Arctic (0–180°W).
767 *Quaternary Science Reviews* 23, 529-560.
- 768 Kaufman, D.S., Schneider, D.P., McKay, N.P., Ammann, C.M., Bradley, R.S., Briffa,
769 K.R., Miller, G.H., Otto-Bliesner, B.L., Overpeck, J.T., Vinther, B.M., 2009. Recent
770 warming reverses long-term arctic cooling. *Science* 325, 1236-1239.
- 771 Keigwin, L.D., Donnelly, J.P., Cook, M.S., Driscoll, N.W., Brigham-Grette, J., 2006.
772 Rapid sea-level rise and Holocene climate in the Chukchi Sea. *Geology* 34, 861-864.
- 773 Kienast, S.S., McKay, J.L., 2001. Sea surface temperatures in the subarctic northeast
774 Pacific reflect millennial - scale climate oscillations during the last 16 kyrs. *Geophys.*
775 *Res. Lett.* 28, 1563-1566.
- 776 Klein, E.S., Nolan, M., McConnell, J., Sigl, M., Cherry, J., Young, J., Welker, J.M.,
777 2015. McCall Glacier record of Arctic climate change: Interpreting a northern Alaska ice
778 core with regional water isotopes. *Quaternary Science Reviews*.
- 779 Köhler, P., Nehrbass-Ahles, C., Schmitt, J., Stocker, T.F., Fischer, H., 2017. A 156 kyr
780 smoothed history of the atmospheric greenhouse gases CO₂, CH₄, and N₂O and their
781 radiative forcing. *Earth System Science Data* 9, 363-387.

- 782 Kokorowski, H., Anderson, P., Mock, C., Lozhkin, A., 2008. A re-evaluation and spatial
783 analysis of evidence for a Younger Dryas climatic reversal in Beringia. *Quaternary*
784 *Science Reviews* 27, 1710-1722.
- 785 Konecky, B., Russell, J., Bijaksana, S., 2016. Glacial aridity in central Indonesia coeval
786 with intensified monsoon circulation. *Earth. Planet. Sci. Lett.* 437, 15-24.
- 787 Kühn, H., Lembke-Jene, L., Gersonde, R., Esper, O., Lamy, F., Arz, H., Kuhn, G.,
788 Tiedemann, R., 2014. Laminated sediments in the Bering Sea reveal atmospheric
789 teleconnections to Greenland climate on millennial to decadal timescales during the last
790 deglaciation. *Climate of the Past* 10, 2215-2236.
- 791 Kurek, J., Cwynar, L.C., Ager, T.A., Abbott, M.B., Edwards, M.E., 2009a. Late
792 Quaternary paleoclimate of western Alaska inferred from fossil chironomids and its
793 relation to vegetation histories. *Quaternary Science Reviews* 28, 799-811.
- 794 Kurek, J., Cwynar, L.C., Vermaire, J.C., 2009b. A late Quaternary paleotemperature
795 record from Hanging Lake, northern Yukon Territory, eastern Beringia. *Quatern. Res.* 72,
796 246-257.
- 797 Lachniet, M.S., Lawson, D.E., Stephen, H., Sloat, A.R., Patterson, W.P., 2016. Isoscapes
798 of $\delta^{18}\text{O}$ and $\delta^2\text{H}$ reveal climatic forcings on Alaska and Yukon precipitation. *Water*
799 *Resour. Res.* 52, 6575-6586.
- 800 Laskar, J., Robutel, P., Joutel, F., Gastineau, M., Correia, A., Levrard, B., 2004. A long-
801 term numerical solution for the insolation quantities of the Earth. *Astronomy &*
802 *Astrophysics* 428, 261-285.
- 803 Li, C., Battisti, D.S., Schrag, D.P., Tziperman, E., 2005. Abrupt climate shifts in
804 Greenland due to displacements of the sea ice edge. *Geophys. Res. Lett.* 32.
- 805 Lisiecki, L.E., Raymo, M.E., 2005. A Pliocene - Pleistocene stack of 57 globally
806 distributed benthic $\delta^{18}\text{O}$ records. *Paleoceanography* 20.
- 807 Liu, Z., Otto-Bliesner, B., He, F., Brady, E., Tomas, R., Clark, P., Carlson, A., Lynch-
808 Stieglitz, J., Curry, W., Brook, E., 2009. Transient simulation of last deglaciation with a
809 new mechanism for Bølling-Allerød warming. *Science* 325, 310-314.

- 810 Liu, Z., Wen, X., Brady, E., Otto-Bliesner, B., Yu, G., Lu, H., Cheng, H., Wang, Y.,
811 Zheng, W., Ding, Y., 2014. Chinese cave records and the East Asia summer monsoon.
812 Quaternary Science Reviews 83, 115-128.
- 813 Livingstone, D., 1955. Some pollen profiles from arctic Alaska. *Ecology*, 587-600.
- 814 Longo, W.M., Huang, Y., Russell, J.M., Morrill, C., Daniels, W.C., Giblin, A.E.,
815 Crowther, J., 2020. Insolation and greenhouse gases drove Holocene winter and spring
816 warming in Arctic Alaska. *Quaternary Science Reviews* 242, 106438.
- 817 Lynch, A., Chapin III, F., Hinzman, L., Wu, W., Lilly, E., Vourlitis, G., Kim, E., 1999.
818 Surface energy balance on the arctic tundra: Measurements and models. *J. Clim.* 12.
- 819 Maier, E., Zhang, X., Abelman, A., Gersonde, R., Mulitza, S., Werner, M., Méheust,
820 M., Ren, J., Chaplignin, B., Meyer, H., Stein, R., Tiedemann, R., Lohmann, G., 2018.
821 North Pacific freshwater events linked to changes in glacial ocean circulation. *Nature*
822 559, 241-245.
- 823 Mangerud, J., Briner, J.P., Goslar, T., Svendsen, J.I., 2017. The Bølling - age Blomvåg
824 Beds, western Norway: implications for the Older Dryas glacial re - advance and the age
825 of the deglaciation. *Boreas* 46, 162-184.
- 826 Manley, W.F., Kaufman, D., 2002. Alaska paleoglacier atlas. Institute of Arctic and
827 Alpine Research (INSTAAR), University of Colorado, Boulder, CO.
- 828 Mann, D.H., Groves, P., Kunz, M.L., Reanier, R.E., Gaglioti, B.V., 2013. Ice-age
829 megafauna in Arctic Alaska: extinction, invasion, survival. *Quaternary Science Reviews*
830 70, 91-108.
- 831 Mann, D.H., Groves, P., Reanier, R.E., Kunz, M.L., 2010. Floodplains, permafrost,
832 cottonwood trees, and peat: What happened the last time climate warmed suddenly in
833 arctic Alaska? *Quaternary Science Reviews* 29, 3812-3830.
- 834 Mann, D.H., Peteet, D.M., Reanier, R.E., Kunz, M.L., 2002. Responses of an arctic
835 landscape to Lateglacial and early Holocene climatic changes: the importance of
836 moisture. *Quaternary Science Reviews* 21, 997-1021.

- 837 Mann, D.H., Reanier, R.E., Peteet, D.M., Kunz, M.L., Johnson, M., 2001. Environmental
838 change and arctic paleoindians. *Arctic Anthropology*, 119-138.
- 839 McManus, J.F., Francois, R., Gherardi, J.M., Keigwin, L.D., Brown-Leger, S., 2004.
840 Collapse and rapid resumption of Atlantic meridional circulation linked to deglacial
841 climate changes. *Nature (London)* 428, 834.
- 842 Melles, M., Brigham-Grette, J., Minyuk, P.S., Nowaczyk, N.R., Wennrich, V., DeConto,
843 R.M., Anderson, P.M., Andreev, A.A., Coletti, A., Cook, T.L., Haltia-Hovi, E.,
844 Kukkonen, M., Lozhkin, A.V., Rosén, P., Tarasov, P., Vogel, H., Wagner, B., 2012. 2.8
845 Million Years of Arctic Climate Change from Lake El'gygytgyn, NE Russia. *Science*
846 337, 315-320.
- 847 Meyer, H., Schirrmeister, L., Yoshikawa, K., Opel, T., Wetterich, S., Hubberten, H.W.,
848 Brown, J., 2010. Permafrost evidence for severe winter cooling during the Younger
849 Dryas in northern Alaska. *Geophys. Res. Lett.* 37.
- 850 Miller, G.H., Alley, R.B., Brigham-Grette, J., Fitzpatrick, J.J., Polyak, L., Serreze, M.C.,
851 White, J.W.C., 2010. Arctic amplification: can the past constrain the future? *Quaternary*
852 *Science Reviews* 29, 1779-1790.
- 853 Okazaki, Y., Timmermann, A., Menviel, L., Harada, N., Abe-Ouchi, A., Chikamoto, M.,
854 Mouchet, A., Asahi, H., 2010. Deepwater formation in the North Pacific during the last
855 glacial termination. *Science* 329, 200-204.
- 856 Oswald, W.W., Brubaker, L.B., Anderson, P.M., 1999. Late Quaternary vegetational
857 history of the Howard Pass area, northwestern Alaska. *Canadian Journal of Botany* 77,
858 570-581.
- 859 Otto-Bliesner, B.L., Brady, E.C., Clauzet, G., Tomas, R., Levis, S., Kothavala, Z., 2006.
860 Last glacial maximum and Holocene climate in CCSM3. *J. Clim.* 19, 2526-2544.
- 861 Pautler, B.G., Reichert, G.-J., Sanborn, P.T., Simpson, M.J., Weijers, J.W., 2014.
862 Comparison of soil derived tetraether membrane lipid distributions and plant-wax δD
863 compositions for reconstruction of Canadian Arctic temperatures. *Palaeogeogr.,*
864 *Palaeoclimatol., Palaeoecol.* 404, 78-88.

- 865 Pendleton, S.L., Ceperley, E.G., Briner, J.P., Kaufman, D.S., Zimmerman, S., 2015.
866 Rapid and early deglaciation in the central Brooks Range, Arctic Alaska. *Geology* 43,
867 419-422.
- 868 Pico, T., Mitrovica, J., Mix, A., 2020. Sea level fingerprinting of the Bering Strait
869 flooding history detects the source of the Younger Dryas climate event. *Science advances*
870 6, eaay2935.
- 871 Porter, T.J., Froese, D.G., Feakins, S.J., Bindeman, I.N., Mahony, M.E., Pautler, B.G.,
872 Reichart, G.-J., Sanborn, P.T., Simpson, M.J., Weijers, J.W.H., 2016. Multiple water
873 isotope proxy reconstruction of extremely low last glacial temperatures in Eastern
874 Beringia (Western Arctic). *Quaternary Science Reviews* 137, 113-125.
- 875 Porter, T.J., Schoenemann, S.W., Davies, L.J., Steig, E.J., Bandara, S., Froese, D.G.,
876 2019. Recent summer warming in northwestern Canada exceeds the Holocene thermal
877 maximum. *Nature communications* 10, 1631.
- 878 Praetorius, S.K., Mix, A.C., 2014. Synchronization of North Pacific and Greenland
879 climates preceded abrupt deglacial warming. *Science* 345, 444-448.
- 880 Putman, A.L., Feng, X., Sonder, L.J., Posmentier, E.S., 2017. Annual variation in event-
881 scale precipitation $\delta^2\text{H}$ at Barrow, AK, reflects vapor source region. *Atmospheric*
882 *chemistry and Physics* 17, 4627-4639.
- 883 Reimer, P.J., Bard, E., Bayliss, A., Beck, J.W., Blackwell, P.G., Bronk Ramsey, C.,
884 Buck, C.E., Cheng, H., Edwards, R.L., Friedrich, M., 2013. *IntCal13 and Marine13*
885 radiocarbon age calibration curves 0-50,000 years cal BP.
- 886 Sachse, D., Billault, I., Bowen, G.J., Chikaraishi, Y., Dawson, T.E., Feakins, S.J.,
887 Freeman, K.H., Magill, C.R., McInerney, F.A., Van der Meer, M.T., 2012. Molecular
888 paleohydrology: interpreting the hydrogen-isotopic composition of lipid biomarkers from
889 photosynthesizing organisms. *Annual Review of Earth and Planetary Sciences* 40, 221-
890 249.
- 891 Sarnthein, M., Kiefer, T., Grootes, P.M., Elderfield, H., Erlenkeuser, H., 2006. Warmings
892 in the far northwestern Pacific promoted pre-Clovis immigration to America during
893 Heinrich event 1. *Geology* 34, 141-144.

- 894 Schmidt, G.A., Bigg, G.R., Rohling, E.J., 1999. Global Seawater Oxygen-18 Database -
895 v1.21.
- 896 Schrag, D.P., Hampt, G., Murray, D.W., 1996. Pore Fluid Constraints on the Temperature
897 and Oxygen Isotopic Composition of the Glacial Ocean. *Science* 272, 1930.
- 898 Serreze, M.C., Holland, M.M., Stroeve, J., 2007. Perspectives on the Arctic's shrinking
899 sea-ice cover. *science* 315, 1533-1536.
- 900 Severinghaus, J.P., Brook, E.J., 1999. Abrupt climate change at the end of the last glacial
901 period inferred from trapped air in polar ice. *Science* 286, 930-934.
- 902 Shah Walter, S.R., Gagnon, A.R., Roberts, M.L., McNichol, A.P., Gaylord, M.C.L.,
903 Klein, E., 2015. Ultra-small graphitization reactors for ultra-microscale ^{14}C analysis at
904 the National Ocean Sciences Accelerator Mass Spectrometry (NOSAMS) Facility.
905 *Radiocarbon* 57, 109-122.
- 906 Shakun, J.D., Carlson, A.E., 2010. A global perspective on Last Glacial Maximum to
907 Holocene climate change. *Quaternary Science Reviews* 29, 1801-1816.
- 908 Stabeno, P.J., Schumacher, J.D., Ohtani, K., 1999. The physical oceanography of the
909 Bering Sea: A summary of physical, chemical, and biological characteristics, and a
910 synopsis of research on the Bering Sea, in: Laughlin, T.R., Ohtani, K. (Eds.), *Dynamics*
911 *of the Bering Sea*. TR Loughlin and K. Ohtani (eds.), North Pacific Marine Science
912 Organization
- 913 Stroeve, J.C., Kattsov, V., Barrett, A., Serreze, M., Pavlova, T., Holland, M., Meier,
914 W.N., 2012. Trends in Arctic sea ice extent from CMIP5, CMIP3 and observations.
915 *Geophys. Res. Lett.* 39.
- 916 Sturm, M., Racine, C., Tape, K., 2001. Climate change: increasing shrub abundance in
917 the Arctic. *Nature* 411, 546-547.
- 918 Tharammal, T., Paul, A., Merkel, U., Noone, D., 2013. Influence of Last Glacial
919 Maximum boundary conditions on the global water isotope distribution in an atmospheric
920 general circulation model. *Climate of the Past* 9, 789.
- 921 Thomas, E.K., Clemens, S.C., Prell, W.L., Herbert, T.D., Huang, Y., Liu, Z., Sinninghe
922 Damsté, J.S., Sun, Y., Wen, X., 2014. Temperature and leaf wax $\delta^2\text{H}$ records

- 923 demonstrate seasonal and regional controls on Asian monsoon proxies. *Geology* 42,
924 1075-1078.
- 925 Thomas, E.K., McGrane, S., Briner, J.P., Huang, Y., 2012. Leaf wax $\delta^2\text{H}$ and varve-
926 thickness climate proxies from proglacial lake sediments, Baffin Island, Arctic Canada. *J.*
927 *Paleolimnol.*, 1-15.
- 928 Tierney, J.E., Zhu, J., King, J., Malevich, S.B., Hakim, G.J., Poulsen, C.J., 2020. Glacial
929 cooling and climate sensitivity revisited. *Nature* 584, 569-573.
- 930 Toolik GIS, 2019. Toolik Field Station Bathymetry, in: Sensing, T.F.S.G.a.R. (Ed.).
- 931 Vachula, R.S., Chipman, M.L., Hu, F.S., 2017. Holocene climatic change in the Alaskan
932 Arctic as inferred from oxygen-isotope and lake-sediment analyses at Wahoo Lake. *The*
933 *Holocene*.
- 934 Vachula, R.S., Huang, Y., Longo, W.M., Dee, S.G., Daniels, W.C., Russell, J.M., 2019.
935 Evidence of Ice Age humans in eastern Beringia suggests early migration to North
936 America. *Quaternary Science Reviews* 205, 35-44.
- 937 Welker, J., 2000. Isotopic ($\delta^{18}\text{O}$) characteristics of weekly precipitation collected across
938 the USA: an initial analysis with application to water source studies. *Hydrological*
939 *Processes* 14, 1449-1464.
- 940 Welker, J.M., 2012. ENSO effects on $\delta^{18}\text{O}$, $\delta^2\text{H}$ and d - excess values in precipitation
941 across the US using a high - density, long - term network (USNIP). *Rapid Commun.*
942 *Mass Spectrom.* 26, 1893-1898.
- 943 Welker, J.M., Rayback, S., Henry, G.H., 2005. Arctic and North Atlantic Oscillation
944 phase changes are recorded in the isotopes ($\delta^{18}\text{O}$ and $\delta^{13}\text{C}$) of *Cassiope tetragona*
945 plants. *Global Change Biol.* 11, 997-1002.
- 946 Wilkie, K., Chaplignin, B., Meyer, H., Burns, S., Petsch, S., Brigham-Grette, J., 2012.
947 Modern isotope hydrology and controls on δD of plant leaf waxes at Lake El'gygytgyn,
948 NE Russia. *Climate of the Past Discussions* 8, 3719-3764.

- 949 Yang, H., Huang, Y., 2003. Preservation of lipid hydrogen isotope ratios in Miocene
950 lacustrine sediments and plant fossils at Clarkia, northern Idaho, USA. *Org. Geochem.*
951 34, 413-423.
- 952 Young, N.E., Briner, J.P., Schaefer, J., Zimmerman, S., Finkel, R.C., 2019. Early
953 Younger Dryas glacier culmination in southern Alaska: Implications for North Atlantic
954 climate change during the last deglaciation. *Geology* 47, 550-554.
- 955 Zimov, S., Zimov, N., Tikhonov, A., Chapin, F., 2012. Mammoth steppe: a high-
956 productivity phenomenon. *Quaternary Science Reviews* 57, 26-45.
957
958
959